J Comput Electron (2006) 5:131–135
DOI 10.1007/s10825-006-8832-3

Atomistic effect of delta doping layer in a 50 nm InP HEMT

N. Seoane · A. J. García-Loureiro · K. Kalna · A. Asenov

Abstract Fluctuations caused by discreteness of charge will play an important role when devices are scaled to gate lengths approaching nanometer dimensions. In this paper, we use a 3D drift-diffusion simulator to study an influence of discrete random dopant charges in the delta doping layer of a 50 nm gate length InP high electron mobility transistor.

Keywords 3D simulation · Parallel solvers · Random dopants · Drift-diffusion · HEMT

1. Introduction

High electron mobility transistors (HEMTs) have been recently scaled to gate lengths approaching nanometer dimensions attaining operating frequencies up to 560 GHz [1]. At these scales, random variations in doping or ternary alloy composition may induce parameter fluctuations which can significantly degrade matching and the RF performance of multifinger devices. The simulation study of these effects require statistical approach running 3D device simulations for a sample of devices with various discrete doping positions where the number and the location of the dopant atoms is different for each particular device in the sample.

In this work, the effect of number of random dopants and their positions in the delta doping layer on device characteristics of a 50 nm gate length InP HEMT with an $In_{0.7}Ga_{0.3}As$ channel has been studied. The study has been carried out with a 3D device simulator based on a drift-diffusion (D-D) transport model using finite element discretisation on an unstructured tetrahedral mesh [2]. Parallel algorithms implementing the Message Passing Interface (MPI) paradigm were used to speed up the whole simulation process and to reduce the computational time necessary for the statistical studies.

The paper is organised as follows. Section 2 describes the main features of our parallel 3D simulator. Results obtained for the simulation of a 50 nm HEMT are presented in Section 3 while conclusions are drawn up in Section 4.

2. Parallel 3D drift-diffusion simulation

Our 3D device simulator is based on the D-D transport model. We have applied the finite element method to discretise the Poisson equation and the electron continuity equation. The meshing is carried out using the QMG program [3]. The resulting tetrahedral mesh is unstructured with more nodes placed below the recesses and the gate of the device, because in these areas we have the greatest gradients of the unknown quantities. To speed up the simulation process the 3D device simulator utilises a parallel approach based on MPI. The METIS program [4] is employed to partition the mesh into sub-domains, so one sub-domain is assigned to each processor.

The discretisation of the D-D system of equations leads to two nonlinear algebraic systems. At each time step, each one

N. Seoane · A. J. García-Loureiro
Department of Electronics and Computer Science, Univ. Santiago de Compostela, Campus Sur, 15706 Santiago de Compostela, Spain

K. Kalna · A. Asenov
Department of Electronics & Electrical Engineering, University of Glasgow, Glasgow, G12 8LT, Scotland, United Kingdom
e–mail: kalna@elec.gla.ac.uk

N. Seoane (✉)
Departamento de Electrónica e Computación, Campus Sur, Universidade de Santiago de Compostela, 15706 Santiago de Compostela, Spain
e-mail: natalia@dec.usc.es

of these nonlinear systems is solved by a Newton–Raphson iterative method. At every step of the Newton method, a linear system $Ax = b$, being A a sparse and non-symmetric matrix, has to be solved. A local linear system of equations is constructed for each sub-domain in parallel manner. Each of these local systems is then solved using domain decomposition methods. If we consider the problem of solving an equation on a domain Ω partitioned in p subdomains Ω_i, such that

$$\Omega = \bigcup_{i=1}^{p} \Omega_i \tag{1}$$

domain decomposition methods attempt to solve the problem on the entire domain by a problem solution on each local subdomain Ω_i.

To solve the linear systems of equations, we have employed the PSPARSLIB library [5]. This library solves sparse linear systems which are distributed over processors. The linear system is first partitioned, then split among the processors according to the partitioning, a distributed data structure is constructed and, finally, a preconditioned Krylov solver is used for its solution.

A detailed analysis of the solution methods and preconditioning techniques employed in PSPARSLIB has been carried out [6], and the lowest execution times were obtained with the Additive Schwarz method. This algorithm is similar to a block–Jacobi iteration and consists of updating all the new components from the same residual. If we assume that A_i is the local matrix of the linear system of equations to be solved on a particular subdomain Ω_i and x_i represents the local solution, the basic Additive Schwarz iteration works as follows:

1. Obtain the external interface nodes $y_{i,ext}$
2. Compute local residual $r_i = (b - Ax)_i$
3. Solve the local linear system $A_i \Delta_i = r_i$
4. Update the solution $x_i = x_i + \Delta_i$

A standard Incomplete LU factorisation with Threshold (ILUT) preconditioner combined with Flexible Generalised Minimal Residual method (FGMRES) is used to solve the linear system $A_i \Delta_i = r_i$ for each of the blocks. More details can be found in [7].

3. Numerical results

The parallel 3D device D-D simulator is applied to study the influence of discrete random dopant charges in the delta doping layer of a 50 nm InP HEMT. The schematic cross-section of the simulated device which consists of a 20 nm Si-doped (10^{19}cm^{-3}) $In_{0.53}Ga_{0.47}As$ cap layer, a 9 nm $In_{0.52}Al_{0.48}As$ etch stop layer, a 4×10^{12} cm^{-2} delta doping layer on top of

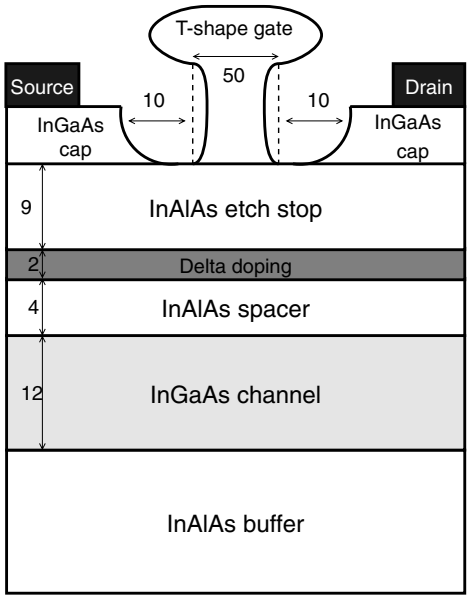

Fig. 1 Cross–section of the 50 nm InP HEMT with the $In_{0.7}Ga_{0.3}As$ channel

an $In_{0.52}Al_{0.48}As$ spacer with a thickness of 4 nm, and a 12 nm $In_{0.7}Ga_{0.3}As$ channel is shown in Fig. 1. The all active device layers are grown on a thick $In_{0.52}Al_{0.48}As$ buffer layer.

The whole study of intrinsic parameter fluctuations is based on a meticulous calibration of the I_D–V_G characteristics of the simulated device at both low and high drain biases of 0.1 V and 0.8 V as shown in Figs. 2 and 3, respectively. Simulated I_D–V_G characteristics have been compared to the measured data obtained from the real 50 nm gate length HEMT as well as to the data obtained from the Monte Carlo (MC) device simulator H2F/MC [8]. Since the parallel 3D D-D device simulator does not allow to include an effect of the surface potential pinning in the recess region, the MC simulations have been performed without interface charge and external resistances.

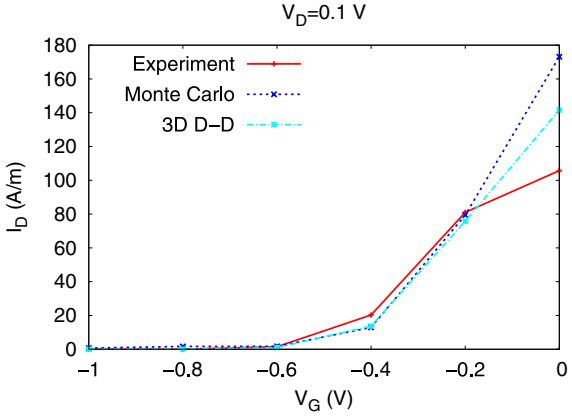

Fig. 2 I_D–V_G characteristics at drain bias of 0.1 V for the 50 nm InP HEMT. Monte Carlo results obtained without the interface charge and external resistance are also shown together with experimental data

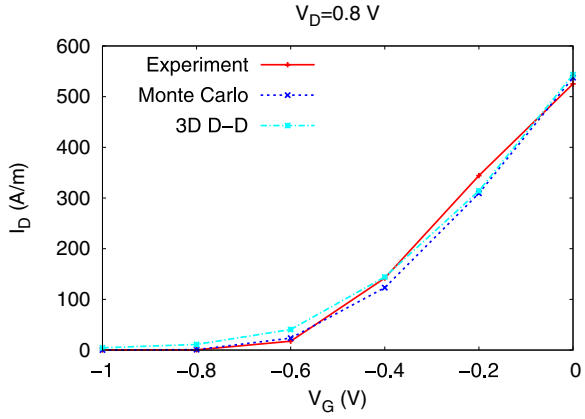

Fig. 3 The same I_D–V_G characteristics as in Fig. 2 but at a drain bias of 0.8 V

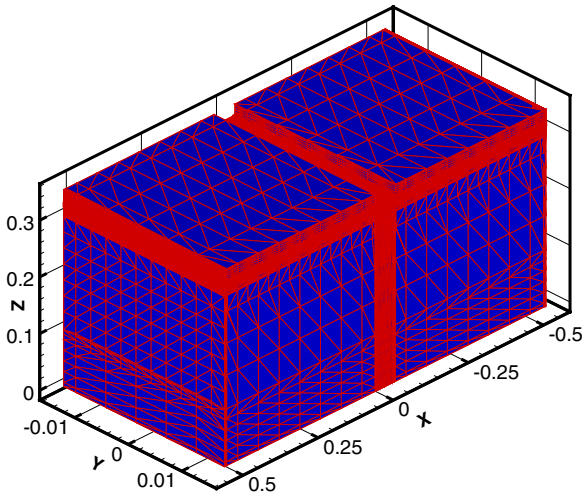

Fig. 5 Tetrahedral mesh of the 50 nm HEMT used to describe the device. The assignments of X, Y and Z-axes are the same as in Fig. 4 geometry

The charge fluctuations in the heavily doped cap layers of the device are assumed to have negligible influence on the channel transport and therefore a continuous doping distribution has been adopted in these regions. The expected number of dopants in the delta doping layer is estimated by using a continuous doping profile to generate the random uniform distribution of the charge. A rejection technique is applied to place the dopants in the 'atomistic' mesh. An internal section view of the random dopants distribution in the delta doping layer is shown in Fig. 4. The extreme values of the 'atomistic' dopant concentration are found below the gate and recesses due to the small size of the elements in these regions as illustrated in Fig. 5. The regions below the gate and recesses affect strongly the current flow along the device channel.

The I_D–V_G characteristics at a low drain bias of 0.1 V and at a high drain bias of 0.8 V for different random dopants distribution (30 configurations) in the delta doping layer are shown in Figs. 6 and 7, respectively. For this calibration,

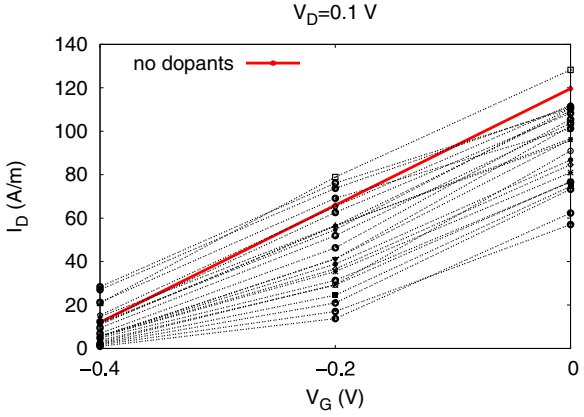

Fig. 6 I_D–V_G characteristics at a drain bias of 0.1 V for different random dopants distributions in the delta doping layer

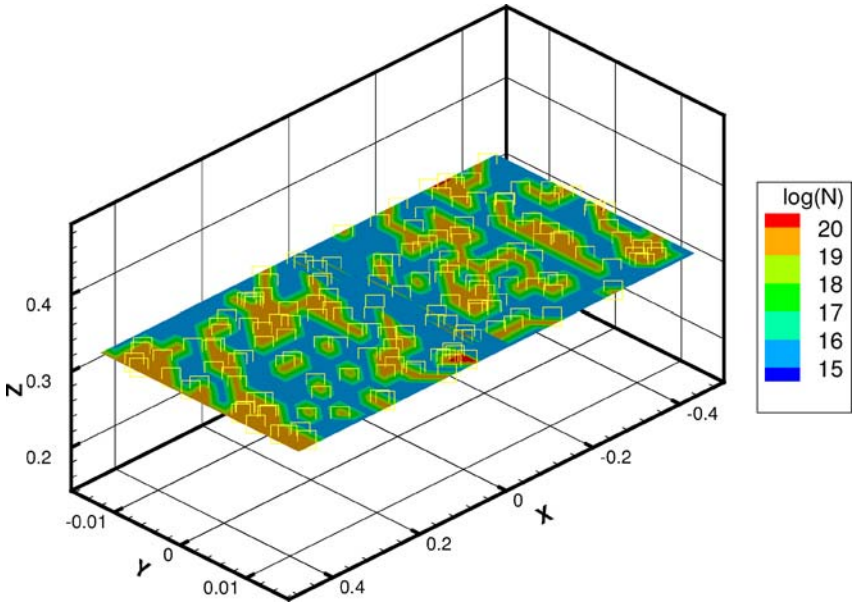

Fig. 4 Example of random dopants distribution inside the delta doping layer. The positions of the dopants are indicated by squares along the plane. The X-axis is along the device with the zero set in the middle of the gate, the Y-axis is along the device depth and the Z-axis is perpendicular to the layers

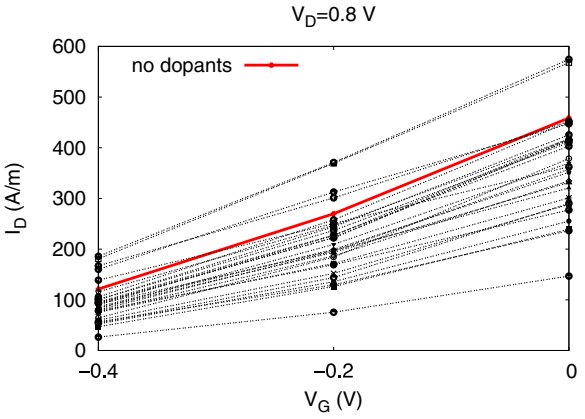

Fig. 7 The same I_D–V_G characteristics as in Fig. 6 but at a drain bias of 0.8 V

a high field mobility model [9], which requires a low field mobility and a saturation velocity as material parameters, has been employed. The low field mobility of 5000 cm^2/Vs and saturation velocity of 4.0×10^7 cm/s have been used for $In_{0.7}Ga_{0.3}$ As channel, and of 3000 cm^2/Vs and 1.0×10^7 cm/s for $In_{0.52}Al_{0.48}$ As layers, respectively.

Statistical parameters, such as the mean value of the drain current, the percentage of drain current fluctuations, the skewness and the kurtosis, characterising the nature of the obtained distributions are shown in Tables 1 and 2. The drain current obtained using a continuous delta doping distribution ($I_{D,cont}$) is also shown for a comparison. The random dopant fluctuations lead, in average, to a lowering of the drain current in HEMTs as demonstrated in Figs. 6 and 7 and calculated in Tables 1 and 2, respectively. We observe a larger lowering of the average drain current at $V_D = 0.1$ V than that at $V_D = 0.8$ V. Charge fluctuations in the delta doping layer, affecting just the electrostatics of a device in our model, have greater influence at small drain current occurring for I_D–V_G characteristics at $V_D = 0.1$ V than at a much larger current observed at a high drain voltage of 0.8 V. This observation is also supported by Tables 1 and 2 where a standard deviation, $\sigma I_D/I_D$, is evaluated for a drain voltage at $V_G = -0.4$, -0.2 and 0.0 V. The standard deviation for the drain current at a low drain voltage of 0.1 V is always larger than the respective standard deviation for the drain current at a high drain voltage of 0.8 V.

Table 1 Statistical parameters characterising the random dopant distribution at $V_D = 0.1$ V

V_G (V)	$I_{D,cont}$ (A/m)	$I_{D,mean}$ (A/m)	$\sigma I_D/I_D$ [%]	Kurtosis	Skew
−0.4	12.023	10.877	77.5	1.168	0.493
−0.2	65.934	49.188	41.9	0.460	−0.111
0.0	119.623	100.820	28.8	1.155	1.273

Table 2 Statistical parameters characterising the random dopant distribution at $V_D = 0.8$ V

V_G (V)	$I_{D,cont}$ (A/m)	$I_{D,mean}$ (A/m)	$\sigma I_D/I_D$ [%]	Kurtosis	Skew
−0.4	121.213	92.279	45.1	0.858	0.296
−0.2	269.752	208.990	34.1	0.580	0.398
0.0	458.786	359.883	26.9	0.218	0.385

4. Conclusions

The parallel 3D device D-D simulator was applied to study the influence of number and random positions of discrete dopant charges in the Si delta doping layer of a 50 nm InP HEMT with a high Indium content channel of 0.7. Since the simulations of random positions of dopants in the delta doping layer are needed for a large set of different devices in order to acquire enough statistical data, the 3D D-D simulator uses finite elements to describe the device mesh and the MPI library to speed up the solutions. The simulated I_D–V_G characteristics indicate that the average drain current obtained in the 50 nm InP HEMTs with randomly positioned delta doping charges is smaller than the equivalent drain current obtained in the device with a continuous delta doping layer. The current lowering is larger at a low drain voltage of 0.1 V compared to the current lowering at a high drain voltage of 0.8 V since the whole effect from different numbers and random positions of discrete delta dopant charges affects only the device electrostatics. The acquired results for different devices have been statistically analysed and main statistical parameters as the mean, the standard deviation, the kurtosis and the skew, were collected in Tables 1 and 2.

Acknowledgments This work was supported by the Spanish Government (CICYT) under the project TIN2004-07797-C02 and by the Project HPC–EUROPA (RII3-CT-2003-506079), with the support of the European Community—Research Infrastructure Action under the FP6 Structuring the European Research Area Programme.

References

1. Yamashita, Y., Endoh, A., Shinohara, K., Hikosaka, K., Matsui, T., Hiyamizu, S., Mimura, T.: Pseudomorphic $In_{0.52}Al_{0.48}As/In_{0.7}Ga_{0.3}As$ HEMTs with an ultrahigh f_t of 562 Ghz, IEEE Electron Device Lett. **23**(10), 573–575 (2002)
2. García Loureiro, A., Kalna, K., Asenov, A.: 3D parallel simulations of fluctuation effects in pHEMTs, J. Comput. Electron. **2**, 369–373 (2003)
3. Vavasis, S. A.: QMG 1.1 reference manual, Computer Science Department, Cornell University (1996)
4. Karypis, G., Kumar, V.: METIS: A software package for partitioning unstructured graphs, University of Minnesota, November (1997)
5. Saad, Y., Lo, G.-C., Kuznetsov, S.: PSPARLIB users manual: A portable library of parallel sparse iterative solvers, Technical report, University of Minnesota (1997)

6. Seoane, N., Loureiro, A. G.: Analysis of parallel numerical libraries to solve the 3D electron continuity equation, *Lecture Notes in Computer Science* **3036**, 590-593 (2004)
7. Loureiro, A.G., Kalna, K., Asenov, A.: Efficient three–dimensional parallel simulations of PHEMTs, *Int. Journal of Numerical Modelling* **18**, 327–340 (2005)
8. Kalna, K., Elgaid, K., Thayne, I., Asenov, A.: Modelling of InP HEMTs with high Indium content channels, Proc. Indium Phosphite and Related Materials, Glasgow 8-12 May (2005), pp. 61–65.
9. Caughey, D. M., Thomas, R. E.: Carrier mobilities in silicon empirically related to doping and fields, Proc. IEEE **55**, 2192-2193 (1967)